The Journal of Experimental Biology 207, 1203-1216
Published by The Company of Biologists 2004
doi:10.1242/jeb.00881

Measurement of cell velocity distributions in populations of motile algae

V. A. Vladimirov[1], M. S. C. Wu[2], T. J. Pedley[3,*], P. V. Denissenko[1] and S. G. Zakhidova[1]

[1]*Department of Mathematics, University of Hull, Cottingham Road, Hull HU6 7RX, UK,* [2]*Department of Biology, Hong Kong University of Science and Technology, Clear Water Bay, Kowloon, Hong Kong* and [3]*Department of Applied Mathematics and Theoretical Physics, University of Cambridge, Wilberforce Road, Cambridge CB3 0WA, UK*

*Author for correspondence (e-mail: tjp3@damtp.cam.ac.uk)

Accepted 10 December 2003

Summary

The self-propulsion of unicellular algae in still ambient fluid is studied using a previously reported laser-based tracking method, supplemented by new tracking software. A few hundred swimming cells are observed simultaneously and the average parameters of the cells' motility are calculated. The time-dependent, two-dimensional distribution of swimming velocities is measured and the three-dimensional distribution is recovered by assuming horizontal isotropy. The mean and variance of the cell turning angle are quantified, to estimate the reorientation time and rotational diffusivity of the bottom-heavy cell. The cells' phototactic and photokinetic responses to the laser light are evaluated. The results are generally consistent both with earlier assumptions about the nature of cell swimming and quantitative measurements, appropriately adjusted. The laser-based tracking method, which makes it possible to average over a large number of motile objects, is shown to be a powerful tool for the study of microorganism motility.

Key words: motility, unicellular algae, *Chlamydomonas nivalis*, laser-based tracking, velocity distribution, swimming direction.

Introduction

Aquatic micro-organisms form a large fraction of the earth's biomass and are of fundamental importance at the bottom of the food chain, both as nourishment for higher links in the chain and, sometimes, as a source of toxicity. Some species are also exploited technologically, for example in bioreactors. Many species are motile, and the swimming behaviour of the cells inevitably has an influence on their interaction with each other and with other species. The understanding of such behaviour and interactions in enough detail to make a useful quantitative prediction of future population levels, in a natural or a man-made environment, requires the use of mathematical models, such as large-scale simulations designed to describe plankton ecology (e.g. Fasham et al., 1990) or very idealised models, designed to highlight particular mechanisms (e.g. Truscott and Brindley, 1995; Matthews and Brindley, 1997).

One class of phenomena for which mathematical modelling is well advanced is spontaneous pattern formation, which has been observed in laboratory suspensions of swimming micro-organisms from a variety of phyla, including algae (Wager, 1911; Kessler, 1985; Bees and Hill, 1997), protozoa (Platt, 1961; Childress et al., 1975) and bacteria (Kessler et al., 1994). The mechanism of pattern formation is a convective one, driven by the up-swimming of cells that are denser than the medium in which they swim, and is called bioconvection (Platt, 1961), the mathematical modelling of which has been discussed by Pedley and Kessler (1992a,b).

An essential ingredient of such mathematical models is a quantitative description of the random swimming behaviour of the cells. For algal cells such as the biflagellate *Chlamydomonas nivalis*, the mechanism for up-swimming in a still fluid is thought to be that the cells are bottom-heavy (Kessler, 1985). The consequence in a moving fluid is that the average orientation of the cells, and hence their swimming direction, is governed by a balance between the gravitational torque and a viscous torque proportional to the vorticity in the ambient flow (called gyrotaxis: see Kessler, 1985).

However, casual observation through a microscope reveals that the trajectories of the cells are intrinsically random, in that different cells swim in randomly different directions and individual cells appear to change direction randomly (though by a small amount at each change) over distances comparable to cell size, the random walks being merely biased by gyrotaxis (Hill and Häder, 1997). Pedley and Kessler (1990) took account of the randomness of the trajectories in their continuum model of suspensions of swimming *C. nivalis* cells. They related the average swimming velocity of the cell (a vector) and the diffusivity to the probability density function (p.d.f.) of the swimming direction, which they assumed to be a random variable independent of the swimming speed. They

also assumed that the p.d.f. of the swimming direction satisfied a particular partial differential equation (a Fokker–Planck, or FP equation), whose form was the same as that was known to be valid for colloidal particles subjected to Brownian rotations. This assumption is consistent with the fundamental theory of random walks (Chandrasekhar, 1943). Although predictions of bioconvection using the model of Pedley and Kessler (1990) agree reasonably well with observation (Bees and Hill, 1997), full confidence cannot be placed in the model without independent experimental confirmation that the trajectories of the cells in an otherwise still fluid are biased random walks, that the p.d.f. of the swimming speed and that of the swimming direction are independent, and that the p.d.f. of the swimming direction satisfies the same FP equation, as assumed by Pedley and Kessler (1990). If all those features are confirmed, then the two unknown parameters occurring in the FP equation (a reorientation time, B, and a rotational diffusivity, D), a pair of constants that can be regarded as indices of that population's swimming behaviour, can be inferred from the data.

Hill and Häder (1997), used a microscope-based tracking method to measure the random trajectories of *C. nivalis*, in an otherwise still fluid, under two sets of conditions: (i) uniform lighting, so that the bias in the random walk was entirely due to gravity, and (ii) illumination from a particular direction, which led to phototaxis coupled with gravitaxis. Trajectories were recorded on video and tracked at time intervals of around 0.08 s, though to avoid errors associated with segments of trajectory being only one or two pixels long, the data had to be sampled at longer time intervals (0.6–3.0 s) and extrapolated back to zero. In the case of gravitaxis, Hill and Häder (1997) found that the data were consistent with the cell motion being a correlated, biased random walk, changing direction apparently continuously, with the mean swimming direction being vertically upwards and the mean swimming speed being 55 $\mu m\ s^{-1}$ (5.5 body lengths per second). Reasonable consistency was also found with the hypothesis that the p.d.f. of the swimming direction satisfied an FP equation of the form proposed by Pedley and Kessler (1990), with a reorientation time B of about 2.7 s and diffusivity D about 0.85 $rad^2\ s^{-1}$ (though the scatter in the data means that these numbers may not be reliable). The microscope-based tracking method was able to view only a few, relatively short trajectories at once, and it was, therefore, a somewhat laborious process to gather enough data for statistical analysis.

In an earlier paper (Vladimirov et al., 2000), the present authors demonstrated the feasibility of a laser-based tracking method, without the use of a microscope, for studying large numbers of trajectories of *C. nivalis* simultaneously. The spatial resolution of the video-recordings was noticeably less fine (1 pixel=20 μm) than that of Hill and Häder (1997; 1 pixel=1.7 μm), and the sampling interval in the method was always more than 1 s. Thus the fine details of the trajectories as the cells continually changed direction were invisible to us, and the results represented averages over the quoted space and time scales. We assumed that Hill and Häder (1997) were correct in identifying the trajectories as correlated, biased random walks, and we show that enough data could be obtained in a short period of time for appropriate averaging to be performed with confidence, so that the method could indeed be used to measure the important properties of populations of swimming cells.

The purpose of the present paper is to apply the laser-based tracking method (with a more automated image processing technique than in Vladimirov et al., 2000) to the measurement of the swimming velocities of many cells in a still fluid in a controlled experimental environment. Statistical analysis of the data is performed to find out whether they are consistent with the hypotheses discussed above: that the cells perform a random walk, that the swimming speed is uncorrelated to the swimming direction (i.e. that the p.d.f. of the swimming velocity is separable into the product of a p.d.f. of speed and a p.d.f. of direction) and that the p.d.f. of direction is close to

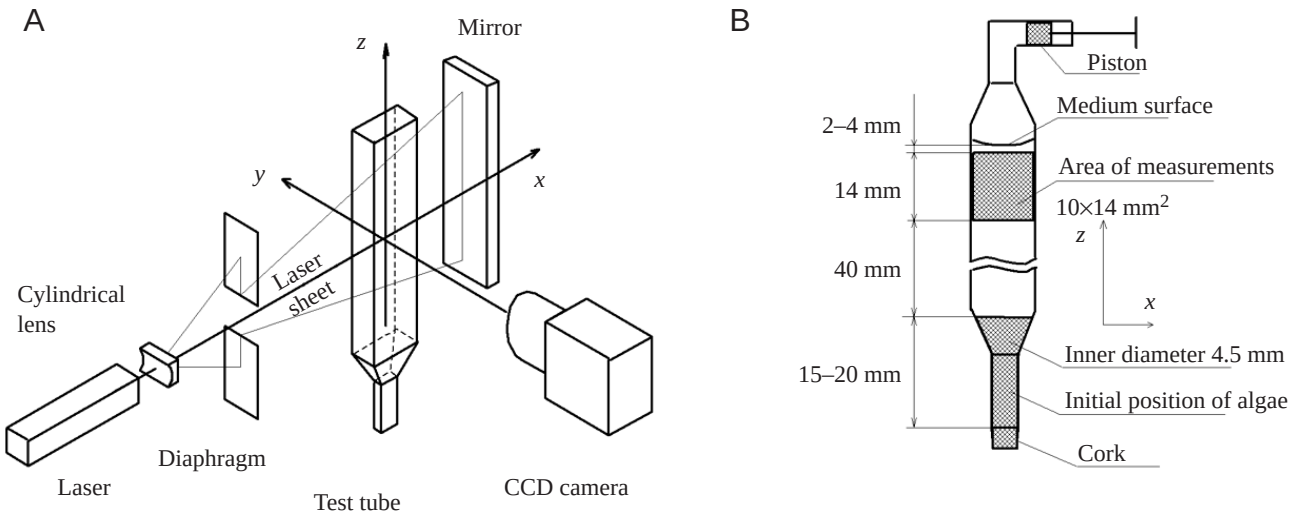

Fig. 1. (A) Experimental setup. (B) Test tube.

the prediction obtained from the gyrotaxis model of Pedley and Kessler (1990). If these hypotheses are consistent, we will be able to estimate the cells' reorientation time and rotational diffusivity, B and D, and compare them with the values obtained by Hill and Häder (1997). The whole experiment is repeated several times, with different batches of cells (though all cultures were of the same age) to test the data for reproducibility. Other closely related questions, such as the influence of the laser light on the cells' swimming, are also studied.

Materials and methods

Algal culture and experimental setup

For the experiments, cultures of the unicellular photosynthetic freshwater flagellate *Chlamydomonas nivalis* (F. A. Bauer) Wille 1903 are used. They are grown by inoculating 1 ml of a logarithmic phase culture into 50 ml of Bold's basal medium + 5% sterilized soil extract. The culture is kept at 23.4°C under a light of about 6000 lux=8.8 W m^{-2} from cool, white-tone fluorescent lights turned on for 16 h a day. Measurements are performed 2 weeks after the inoculation of the culture. Microscopic observation shows that the diameter of an individual cell in these cultures lies in the range 3–5 μm.

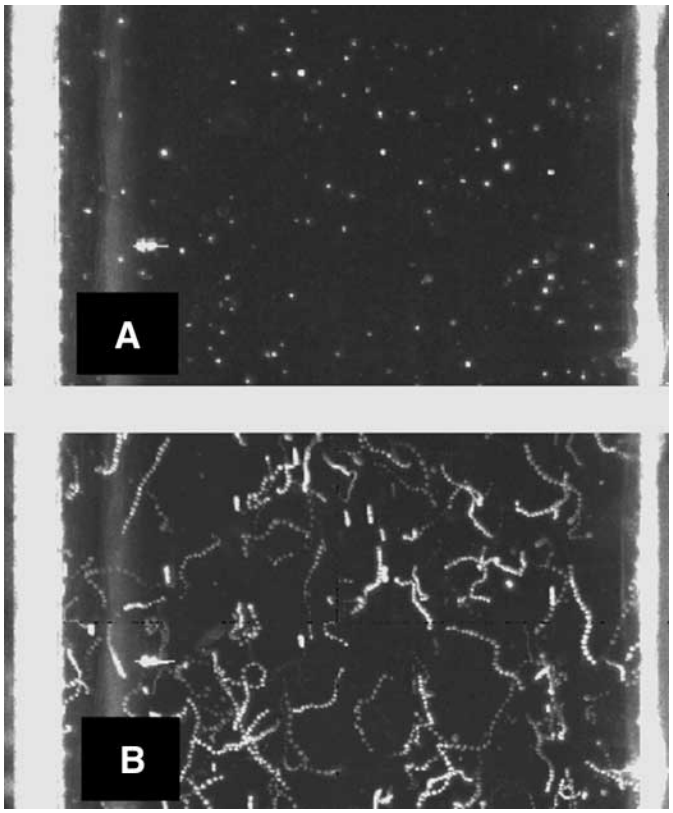

Fig. 2. (A) Typical image of swimming cells. The white vertical bars represent the walls of the test tube, which is 1 cm wide. (B) Composite image from the 21 images acquired in a burst: algal tracks are clearly seen; the short straight vertical tracks are made by sedimenting dust particles.

The experimental setup used is generally similar to the one described in Vladimirov et al. (2000), see Fig. 1A. An argon ion laser with a wavelength of 514 nm (green) and light intensity of 1400 W m^{-2} is the only light source in the experiments. Laser light passes through a cylindrical lens and a diaphragm, which produces a vertically oriented light sheet with a cross-section of 14 mm×1.5 mm. The laser sheet is directed along the plane of symmetry of the vertically positioned test tube of rectangular cross-section (Fig. 1B) containing medium and algal cells. A mirror is placed behind the test tube to make the cells' illumination symmetric, thus avoiding bias in their self-swimming. Images are acquired with a Kodak Megaplus 1.4 CCD camera, resolution of 1316×1034 $pixels^2$. The laser, optical system and acquisition system belong to a Particle Image Velocimetry (PIV) System (TSI Inc., Shoreview, MN, USA).

To describe the results, a Cartesian coordinate system is used with axes (x,y,z) directed as shown in Fig. 1A. The projection of the cells' displacements (or velocities) onto the x–z plane is recorded. The measurement volume (with x,y,z sizes of 10 mm×1.5 mm×14 mm) represents the intersection of the laser sheet with the test tube. The depth of the measurement area, that is the thickness of the laser sheet of 1.5 mm, is twice as large as the distance that a typical cell can travel in 30 s.

Experimental procedure

To observe the algal cells' self-swimming in the still fluid, the following experimental procedure is carried out.

(1) The test tube (Fig. 1B) is filled with the medium in which the culture was grown, after filtration (average filter pore size is 0.45 μm). Filtration decreases the number of sediment

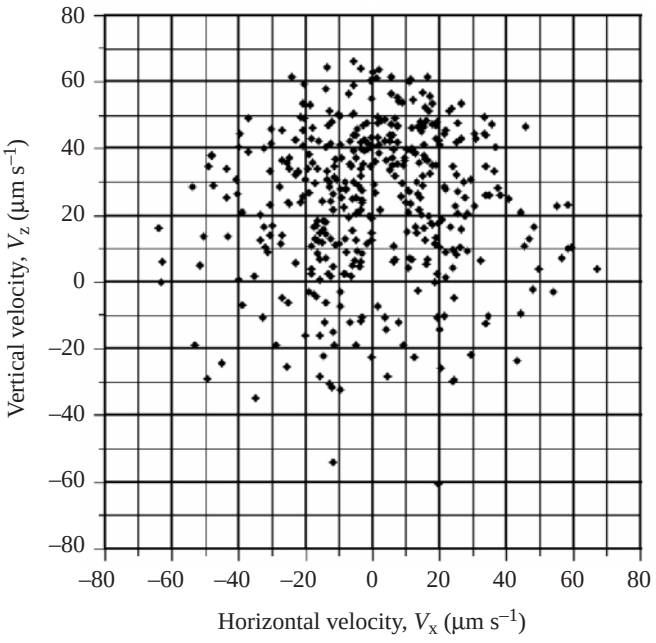

Fig. 3. Typical scatter plot of vertical and horizontal velocities of the cells detected within a burst. Cells clearly swim upwards on average.

particles in the medium (dust, dead cells etc.) that confuse recognition of live cells.

(2) The test tube is left in a vertical position for approx. 15 min to allow the initial temperature and velocity perturbations in the medium to decay.

(3) The lower (open) end of the test tube is submerged into the medium containing the algal culture, which is sucked into the lower section of the test tube by slow withdrawal of a piston at a speed of approx. 1 mm s^{-1}, and the bottom of the test tube blocked with a cork (Fig. 1B).

(4) The test tube is placed into the working position (Fig. 1B). The cells are now located near the bottom of the test tube. The time instant at which this is done is t=0 for each experiment.

(5) The test tube is placed inside a larger rectangular vessel (100 mm×100 mm×220 mm) filled with distilled water at a stabilized temperature of 23.4°C. This provides a water jacket around the test tube in order to diminish temperature gradients and, hence, thermal convection in the test tube that may be generated by either laser heating or environmental perturbations.

(6) After approx. 15 min, the first 20–25 cells cover the distance between their initial position and the lower edge of the measurement area (40 mm) (Fig. 1B); the laser is then turned on and the CCD camera acquires 21 images (‘frames’) of exposure time 0.256 s, separated by an interval δt of 1.1 s. A fragment of a typical frame is shown in Fig. 2A. Each set of 21 successive frames is denoted as a ‘burst’. After a burst is acquired, the laser is turned off for a few minutes until the next burst is started. Bursts obtained during one experiment form an experimental ‘run’.

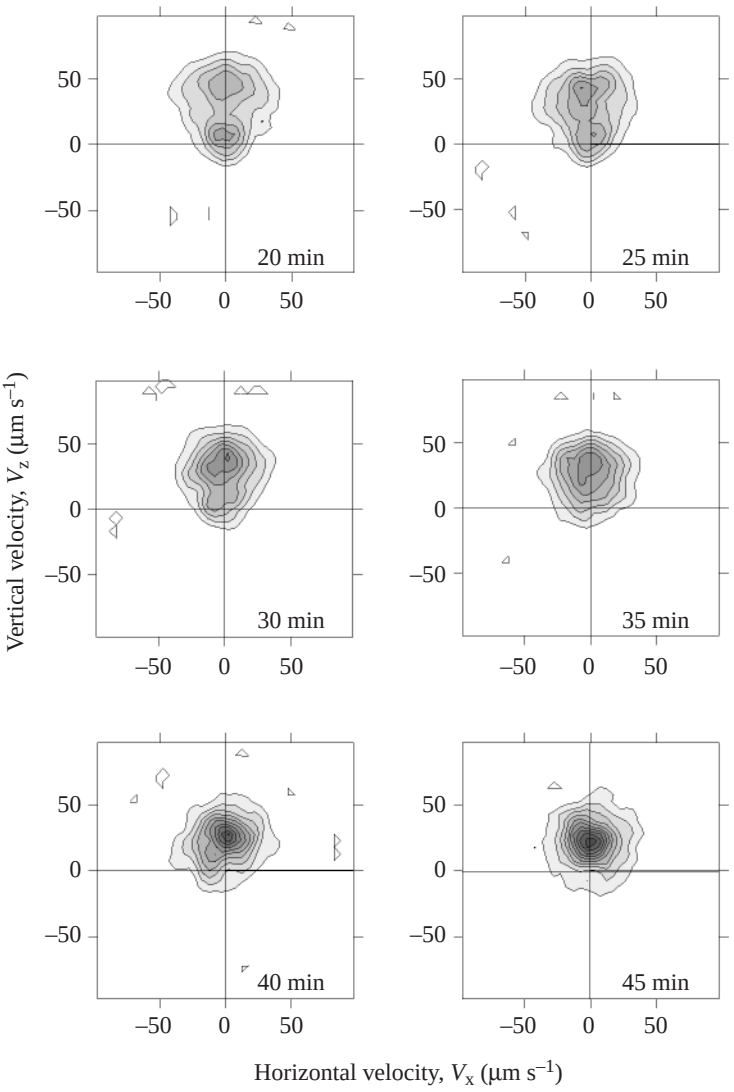

Fig. 4. Time evolution of the cells’ distribution by two-dimensional projections of velocities onto x–z plane. Contour plots of the probability density function (see Equation 5) at six time instants. The difference between colour levels is 0.00015 s^2 μm^{-2}. In the 20 min plot, where the number of motile cells that had reached the observation area is small, the peak corresponding to suspended dust particles is seen. On later images, where the number of active swimmers is large enough, this peak vanishes.

Cell tracking

Now we have a number of 21-image sets (bursts), from which the cells’ velocities are to be recovered. Most of the bright blobs in Fig. 2A correspond to swimming algal cells. These blobs have sizes from 1×1–3×3 $pixels^2$, while the camera resolution is 1 pixel=20 μm. Thus, the size and shape of a blob do not match the actual size and shape of a cell and depend only on the amount of light scattered by it.

To get a visual impression of the cells’ behaviour, we assign the brightness of each pixel *(x,z)* to be the largest brightness met among the 21 images of a burst at the location *(x,z)*, to obtain an image of the tracks of the swimming cells (Fig. 2B). The several short vertical tracks correspond to dust particles suspended in the medium. The lengths of these tracks give an estimate of the typical distance travelled by dust particles during one burst (21 s) due to either motion of the medium or their own sedimentation under gravity.

To obtain values of the swimming cells’ velocities, tracking software has been created using C++ in a UNIX environment. The code analyzes image sets (bursts), identifies bright blobs on each image and calculates the coordinates of each cell as the weighted centre of mass of the corresponding grey-valued blob. Then the tracks are reconstructed by searching for the most probable position of the cell among the blobs detected in the frame n+1, given the cell’s position and velocity in the frame n. To find the best candidate for the track continuation, we minimize the linear combination:

$$C_1\left|\frac{b_{n+1}-b_n}{\sqrt{b_{n+1}b_n}}\right| + C_2\left|\frac{v_{n+1}-v_n}{\sqrt{v_{n+1}v_n}}\right| + C_3\left(1-\left|\frac{\vec{v}_{n+1}-\vec{v}_n}{\sqrt{v_{n+1}v_n}}\right|\right), \quad (1)$$

where b_n, b_{n+1} is the brightness of the blob interpreted as the cell image in frames n and n+1 and $\vec{v}$ is the cell velocity derived from the difference of its position in sequential images (v_n is

the magnitude of the velocity vector $\vec{v}_n$). Thus, blob chains with a not-too-sudden change in the blob's brightness (1st term), a not-too-sudden change in the speed between two sequential blobs (2nd term) and not-too-sharp angles (3rd term) are interpreted as the cell trajectories. The coefficients C_1, C_2, C_3 are tuned empirically by visual comparison of reconstructed tracks with images similar to Fig. 2B.

To diminish the error related to inaccuracy in the measurement of the cells' positions, triple displacements of the cells (i.e. the displacement between frame n and n+3, for any n) are used to calculate velocities. The results obtained by considering single and double displacements turned out to be too noisy. Finally, each burst gives an array of sets of $(V_x, V_z)_n$ which represent sequential cells' instantaneous velocities within a track. A typical set of $(V_x, V_z)_1$ pairs corresponding to the cell displacement from the 1st to the 4th point of its track is presented graphically in Fig. 3 as a 'cloud of points', where each point corresponds to the velocity of an individual cell.

Background velocity of the medium

This study is devoted to the cells' swimming in a still fluid, so it was essential to minimize velocity of the ambient medium and ensure that it is well below a typical speed of cell swimming of tens of micrometres per second. Estimates show that the characteristic time of viscous decay of the velocity perturbations in the test tube is 10 s and thus the initial velocity perturbation of about 1 cm s^{-1} decays to 10 μm s^{-1} in about 1 min. So velocity perturbations arising from manipulations of the test tube can be neglected.

Another source of the medium motion is bioconvection arising from spatial variation in the cells' concentration leading to a variation in the average fluid density, which would drive the convective motion. A force balance between gravity (buoyancy) and the viscous force yields the result that to cause bioconvection with a speed of 10 μm s^{-1}, a relative variation of fluid density of 10^{-7} is required, and that corresponds to a variation in the number density of cells of the order of 10 mm^{-3}. The total cell concentration is not more than 1 mm^{-3} in our experiments, so that its variation is even less and no bioconvection can arise. In comparison, the typical cell concentration in the experiments by Kessler (1986) and Bees and Hill (1997), where the existence of bioconvection is apparent, is around 1000 mm^{-3}.

The third source of motion of the ambient medium is density variation due to temperature variation caused by either laser radiation or some other source, e.g. the test tube being heated by the experimenter's hands. Experiments show that the laser radiation does not cause thermal convection. To estimate the influence of initial temperature perturbations, an argument similar to that used in the context of bioconvection shows that a relative fluid density variation of 10^{-7} can drive convective motion of 10 μm s^{-1}. To cause a relative density variation of 10^{-7}, however, a temperature variation of 4×10^{-4} K is necessary. The estimates show that approx. 10 min is required for a temperature variation of 1 K to decay below this value. This time interval is comparable with the experimental run duration and that is why the test tube is placed in the water jacket, providing a uniform temperature along it.

Statistical analysis and results

Cells' velocity distribution

To obtain the instantaneous distribution of cells by velocity, the two-dimensional velocity space (V_x,V_z) is subdivided into square bins of width ΔV=10 μm s^{-1}, so that a velocity (V_x,V_z) is placed in bin (i,j) if:

$$i\Delta V < V_x < (i+1)\Delta V\,; \quad j\Delta V < V_z < (j+1)\Delta V\,, \quad (i, j = -10\ldots10)\,. \quad (2)$$

Let $n_{r,b,ij}$ be the number of cells with velocity in the bin (i,j) detected during burst b of run r, and $N_{r,b}=\sum_{i,j}n_{r,b,ij}$ be the total number of cells detected in the burst b of run r. Then, the instantaneous distribution $F_{r,b,ij}$ of cells by their swimming velocities measured at the time instant $t_{r,b}$ is defined as:

$$F_{r,b,ij} = n_{r,b,ij} / N_{r,b}\,. \quad (3)$$

In fact, $t_{r,b}$ is defined with a precision of 22 s, that is the duration of a burst. In order to compare runs with each other, a continuous function of time $F_{r,ij}(\tau)$ is introduced. It is constructed by linear interpolation between successive bursts b and b+1 of each run r:

$$F_{r,ij}(\tau) = \frac{(t_{r,b+1}-\tau)F_{r,b,ij} + (\tau - t_{r,b})F_{r,b+1,ij}}{t_{r,b+1}-t_{r,b}}, \quad (4)$$

where τ belongs to the time interval $(t_{r,b}, t_{r,b+1})$. The procedure (Equation 4) preserves the norm condition $\sum F_{r,ij}$=1. Now, the weighted average of $F_{r,ij}$ over all runs is defined as:

$$\bar{F}_{ij}(\tau) = \frac{1}{\sum_r w_r(\tau)} \sum_m F_{r,ij}(\tau) w_r(\tau)\,, \quad (5)$$

where $w_r(\tau)$ is the weight proportional to the number of cells detected in the corresponding run:

$$w_r(\tau) = \frac{(t_{r,b+1}-\tau)N_{r,b} + (\tau - t_{r,b})N_{r,b+1}}{t_{r,b+1}-t_{r,b}}\,. \quad (6)$$

The function $\bar{F}_{ij}(\tau)$ is considered as a presumptive p.d.f. of the cells' velocity distribution and this assumption is tested below (see Appendix). Function $\bar{F}_{ij}(\tau)$ is associated with a continuous function of three variables $\bar{F}(V_x,V_z,\tau)$, of which a contour plot is presented in Fig. 4 for several time instants.

Reconstruction of the three-dimensional velocity distribution

The measured cells' swimming velocities are the two-dimensional projections of the actual three-dimensional velocities. However, the cells' motion and most of the models describing it are three-dimensional. Thus it is important to recover the three-dimensional distribution. Reconstruction of the three-dimensional p.d.f. $f(V_x,V_y,V_z)$ from a measured

projection $F(V_x,V_z)$ is feasible if $f(V_x,V_y,V_z)$ is assumed to be axially symmetric, i.e. if the cells are equally likely to swim in any horizontal direction. In cylindrical coordinates (r,ϕ,z) with the z axis directed vertically upwards, an axially symmetric p.d.f. $f(V_x,V_y,V_z)$ can be represented as $f(V_r,V_z)$, where $V_r=\sqrt{V_x^2+V_y^2}$ is the horizontal velocity component. Since $F(V_x,V_z)$ is the two-dimensional projection of $f(V_r,V_z)$,

$$F(V_x,V_z) = \int_{-\infty}^{+\infty} f\left(\sqrt{V_x^2+V_y^2},V_z\right) dV_y \qquad (7)$$

or after a change of variables,

$$F(V_x,V_z) = 2\int_{V_x}^{+\infty} \frac{f(V_r,V_z)V_r}{\sqrt{V_r^2-V_x^2}}\, dV_r\,. \qquad (8)$$

This equation is known as the Abel Integral Equation for $f(V_r,V_z)$. According to Gorenflo and Vessela (1991), the solution of this equation is given by:

$$f(V_r,V_z) = -\frac{1}{\pi}\int_{V_r}^{+\infty} \frac{\partial}{\partial V_x}\frac{F(V_x,V_z)}{\sqrt{V_x^2-V_r^2}}\, dV_x\,. \qquad (9)$$

This integral is here evaluated numerically with the use of the discrete representation of $F(V_x,V_z)$ as $\bar{F}_{ij}$, as defined in Equation 5. Surface plots of reconstructed distributions $f(V_r,V_z)$ at several time instants are presented in Fig. 5. For convenience, variables $V=\sqrt{V_r^2+V_z^2}$ (the cell forward velocity) and $\theta=\mathrm{atan}(V_r/V_z)$ (the angle between the trajectory and the vertical) are used instead of V_r and V_z.

Evolution of the averaged parameters of cells' self-swimming

The mean of the vertical, horizontal, and absolute projected velocities, $\langle V_z\rangle_{r,b}$, $\langle V_x\rangle_{r,b}$ and $\langle V_p\rangle_{r,b}=\langle\sqrt{V_z^2+V_x^2}\rangle_{r,b}$, and their standard deviations are calculated for all cells detected in each burst b of each run r. Substituting $\langle V_z\rangle_{r,b}$, $\langle V_x\rangle_{r,b}$ and $\langle V_p\rangle_{r,b}$ into Equations 4 and 5 instead of $F_{r,b,ij}$, we obtain weighted averages $\bar{V}_z(\tau)$, $\bar{V}_x(\tau)$, $\bar{V}_p(\tau)$, over all runs. The results are presented in Fig. 6A: values of $\langle V_z\rangle_{r,b}$, $\langle V_x\rangle_{r,b}$ and $\langle V_p\rangle_{r,b}$ are plotted as diamonds and the averaged values $\bar{V}_z(\tau)$, $\bar{V}_x(\tau)$, $\bar{V}_p(\tau)$ are plotted as solid lines. Standard deviations of cell velocity obtained in a similar way are plotted in Fig. 6B. Both the mean values and standard deviations decrease as the slower swimming cells reach the observation area.

To illustrate the inhomogeneity of cells' motility across the camera field of view, the observation area is divided into quarters and the averaged velocities $\bar{V}_z(\tau)$, $\bar{V}_x(\tau)$, $\bar{V}_p(\tau)$ are calculated separately for each quarter (Fig. 7). Cells located in the upper half of the camera's field of view (furthest from the injection point) are observed to swim faster than those located in the lower part, while cells in the left and right halves (closer to and further from the laser, respectively) appear to be similar.

To check if the laser light affects cells' motility in our experimental arrangement, we compare averaged parameters based on the data taken from the 1...6, 3...9, 6...12, 9...15, 12...18, 15...21st

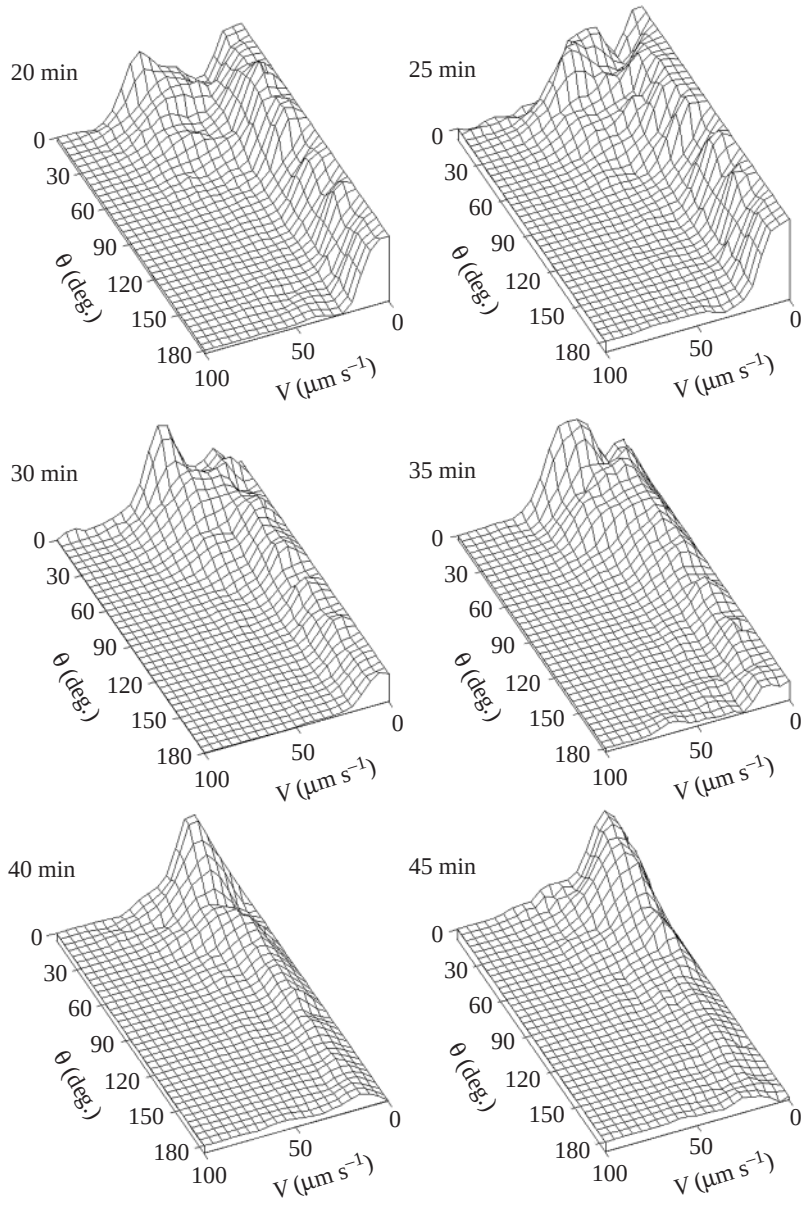

Fig. 5. Time evolution of the three-dimensional cells' distribution by velocities. Surface plot of reconstructed three-dimensional probability density function $f(V_r,V_z)$ (Equation 9), expressed as $f(V,\theta)$, at six time instants. The axes correspond to the cell absolute velocity $V=\sqrt{V_r^2+V_z^2}$ and the cell velocity angle to the vertical $\theta=\mathrm{atan}(V_r/V_z)$. A maximum observed at small V is related to the passive particles suspended in the medium. At about 40 min the number of active swimmers in the observation area becomes large compared to that of passive particles and this maximum vanishes.

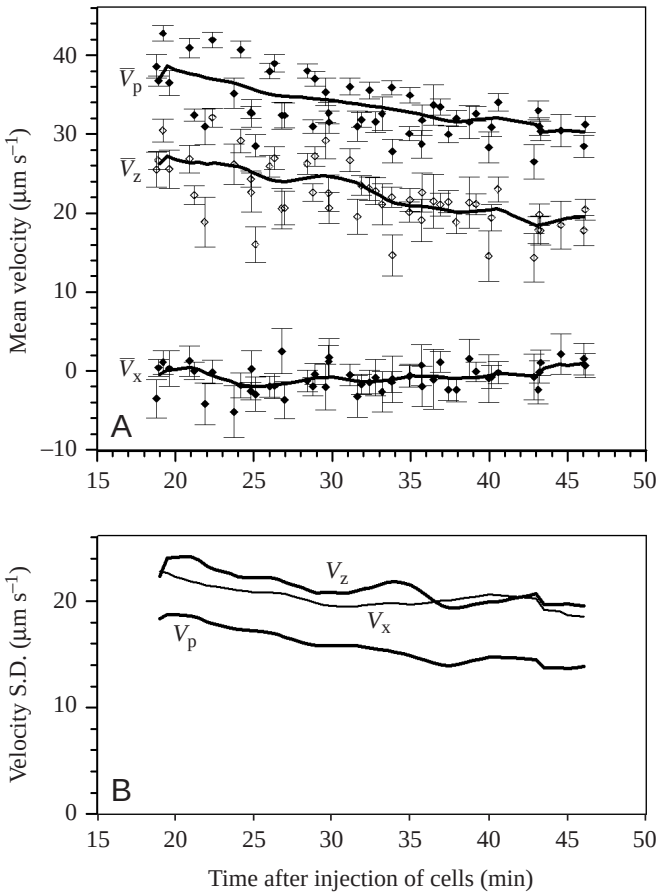

Fig. 6. Time evolution of averaged velocities (A) and their standard deviations (B) for the cells located in the camera field of view. Absolute projected velocity V_p, vertical velocity V_z and horizontal velocity V_x. Diamonds with error bars correspond to the instant values $\langle V_x\rangle_{r,b}$, $\langle V_z\rangle_{r,b}$, $\langle V_p\rangle_{r,b}$. Solid lines correspond to averaged values of V_p, V_z and V_x in A and to their standard deviations in B, obtained using an equation similar to Equation 5.

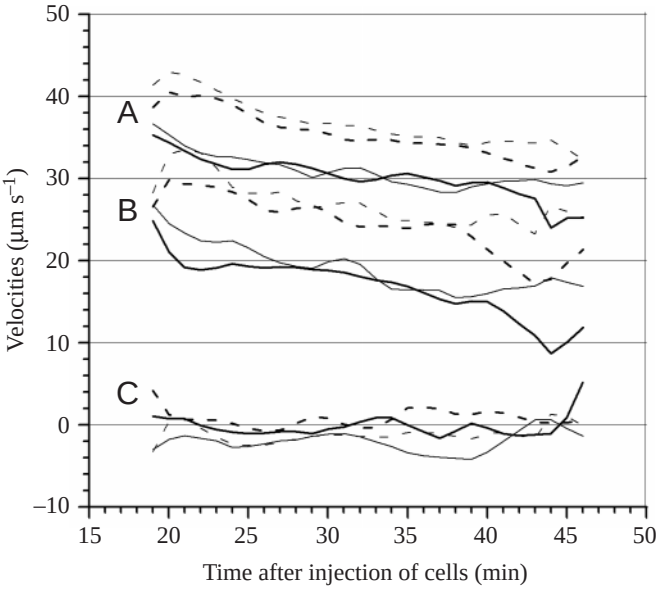

Fig. 7. Averaged (A) absolute projected velocity V_p, (B) vertical velocity V_z and (C) horizontal velocity V_x, calculated separately for the tracks detected in the different quarters of the observation area (compare with Fig. 6). Broken bold lines correspond to the upper right quarter, broken thin line to the upper left quarter, solid bold line to the lower right quarter and solid thin line to the lower left quarter of the observation area. As expected, faster swimmers (ones with higher vertical and projected velocities) are located further from the injection point at the bottom of the test tube.

frames within each burst, i.e. at approximately 3, 6, 9, 12, 15 and 18 s after the burst starts. Mean horizontal, vertical and absolute projected velocities calculated in the same way as for Fig. 6 are plotted in Fig. 8A and the standard deviations of V_z and V_p are plotted in Fig. 8B. The data related to 18 s, 15 s, 12 s, 9 s, 6 s, 3 s are shown by lines of descending thickness, so that the boldest line corresponds to 18 s and the thinnest line to 3 s. The symbols correspond to the data obtained at high laser light intensity and will be discussed later. Observe that the three thin lines are very close to each other, which means that a photokinetic response (cell acceleration) starts to develop only after the first 10 s of laser illumination.

Parameters for the entire cell population

In previous sections the time-dependence of the cells' velocity distribution has been considered. One reason for the time-dependence is that we only deal with the motion of cells located in the camera field of view at the time instant $t_{r,b}$. However, to model the behaviour of an entire system, for example to model bioconvection, it is essential to know the properties of the population as a whole. A variety of methods are used to obtain the population properties from the measured time-dependent values $\overline{F}(t)$,$\overline{V}_z(t)$, $\overline{V}_x(t)$ and $\overline{V}_p(t)$. Each method has its advantages and disadvantages, so the most straightforward one is chosen, namely, the cells' velocity distribution based on all tracks detected during all experimental runs is calculated as if all tracks were detected during one burst.

The distributions for V_x, V_y and V_p are shown in Fig. 9. The one-dimensional angular distribution $f(\theta)$ is obtained from the three-dimensional p.d.f. $f(V,\theta)$ reconstructed in accordance with Equation 9. The average horizontal velocity V_x calculated over the whole population is $-1.7\ \mu m\ s^{-1}$, the average vertical velocity V_z is $26\ \mu m\ s^{-1}$, the average projected velocity V_p is $38\ \mu m\ s^{-1}$. The two-dimensional and reconstructed three-dimensional probability density functions of the velocity distribution for the entire cell population are shown in Fig. 10 on linear and logarithmic scales.

Discussion

Laser-based cell tracking has been applied to study the motility of the unicellular algae *Chlamydomonas nivalis*. The technique enables observation of up to several hundred cells simultaneously and provides ample material for investigation into the general statistical properties of the cell self-propulsion

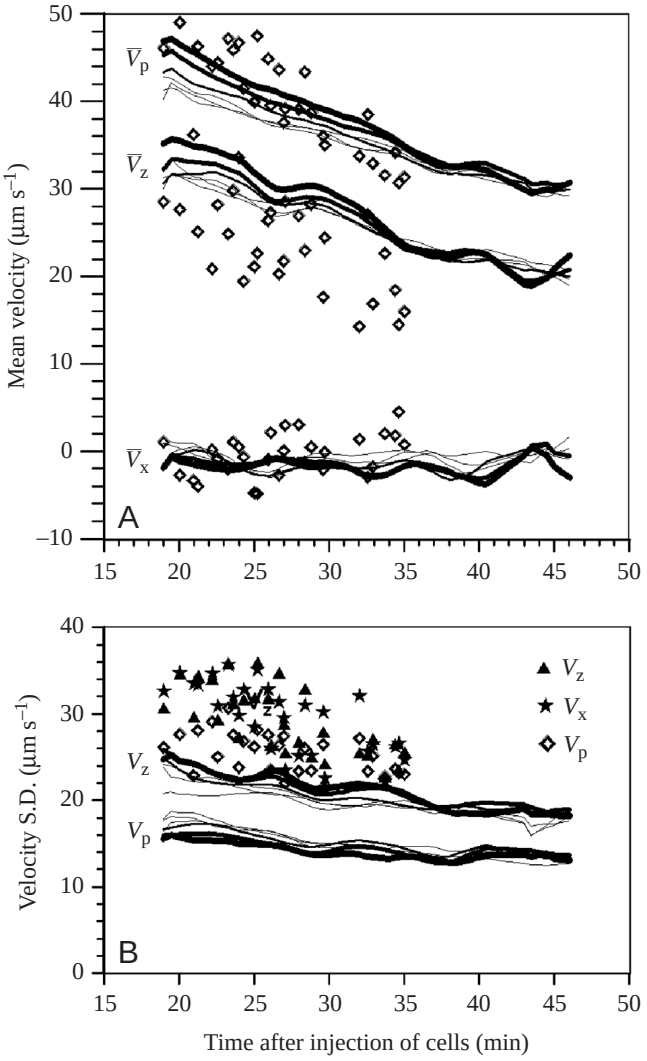

Fig. 8. Average parameters based on different parts of tracks (compare with Fig. 6). Thin lines correspond to data based on the four-point track fragments from frames 4–6, 6–9, 9–12 of the bursts; thicker lines correspond to frames 12–15, 15–18, 18–21 (boldest). Observe that the three thin lines indicating mean velocities almost coincide, i.e. the photokinetic response starts to develop around 10 s after the laser is switched on. The symbols correspond to the average parameters measured in the runs with laser intensity ten times higher than in the standard experiments.

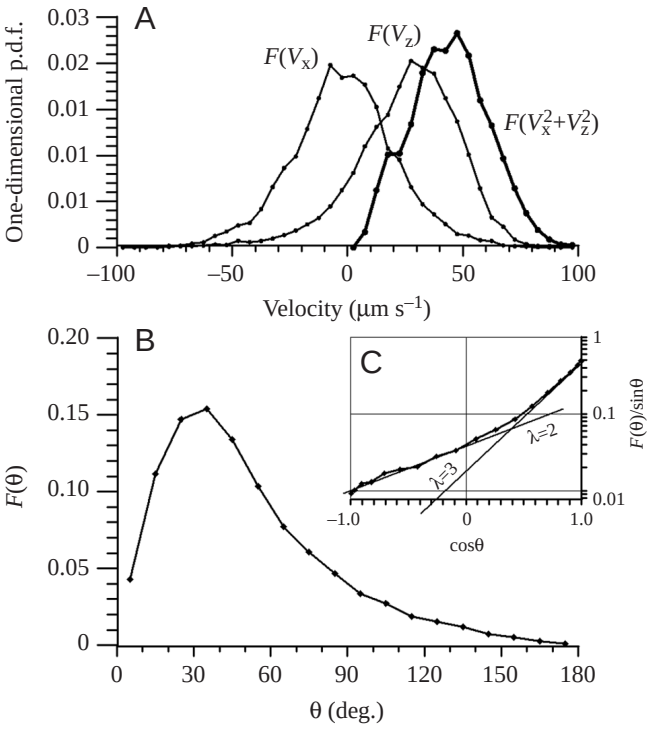

Fig. 9. One-dimensional distributions based on analysis of all tracks detected in all runs. (A) Distributions of cells by V_x, V_z and V_p; (B) cells' distribution by swimming direction θ=atan (V_r/V_z), obtained from the three-dimensional axisymmetric distribution reconstructed in accordance with Equation 9; (C) cells' distribution by θ plotted in B divided by sinθ, i.e. $\int_0^\infty f[V_r(V,\theta),V_z(V,\theta)]V^2 dV$ *versus* cosθ. The slope of this graph corresponds to values of λ in the Fisher distribution (Equation 10) in the range 2–3.

and the time evolution of cell motility. An experimental protocol, providing repeatable delivery of motile cells to the observation area and a technique for the simultaneous tracking of up to a few hundred cells located in the observation area are developed.

In particular, the medium containing the algal cell culture is injected into the bottom of the test tube a few cm below the section visible by camera. The cells gradually reach the observation area, where their trajectories are recorded. The time evolution of the average parameters of cells located in the observation area is fairly repeatable, though one of the eight experimental runs appeared to be invalid: the distribution functions $F_{ij}(\tau)$ calculated in accordance with Equation 5 on the basis of all eight experimental runs failed to pass the goodness-of-fit test. On separate examination, one run was found to be noticeably different from the others. This inconsistent run was eliminated and the distribution function $F_{ij}(\tau)$ calculated on the basis of the seven remaining runs passed the test successfully (see Appendix).

The decrease of the average cell velocities with time (Fig. 6) corresponds to the natural variability of cell motility within the population. Indeed, if all the cells were exactly the same, the time taken to reach the camera's field of view would be different only due to statistical scatter, and the average parameters of the cells located in the observation area would be independent of time, as happens, for example, when sedimentation of identical Brownian particles is observed (Nikolai et al., 1975). In turn, if a population consists of differently swimming cells, faster swimmers generally reach the camera field of view earlier than the slower ones, and the average cell velocities at the beginning of a run are higher than at the end, in agreement with the data shown in Fig. 7; indeed, cells in the upper parts of the measurement area tend to have a higher speed than those in the lower part.

Influence of the laser light on cell motility

Chlamydomonas nivalis is a photo-responding alga. When it is illuminated steadily from a particular direction, it tends to swim towards or away from the light source, depending on the light intensity (phototaxis). Photophobic (for example, Matsunaga et al., 1999) and photokinetic effects can also occur, i.e. the cell stops swimming, decelerates or accelerates after the lighting conditions are changed.

In our experiments, the laser is the only source of light illuminating the cells. Its wavelength, 514 nm, is in the range to which *C. nivalis* is known to respond (Harris, 1989, p. 211; this interval is approximately 475–575 nm). Moreover, the light intensity used for the measurements (1400 W m^{-2}) is twice as high as the maximum sunlight intensity on the Earth's surface and 200 times higher than that in the light-shelf where the cells are grown. To diminish the cells' phototactic response, a mirror is placed behind the test tube forming a back-propagating laser sheet, thus making the cells' illumination more symmetric (Fig. 1). The laser is switched on only during a burst (22 s) for image acquisition and switched off for several minutes between bursts, so that most of the time the cells swim in darkness. Since a light response normally needs time to develop (Kessler et al., 1992), the question is whether the 22 s of illumination is enough to cause any response. Fig. 8 shows that the photokinetic response starts to develop around 10 s after the laser is switched on. Thus, images from the first halves of bursts can be used without worrying about the influence of the laser light.

To study the influence of the laser light on the cells' motility, the same protocol was used as for a standard run, but the cells were illuminated with a higher laser light intensity. Several experimental runs with the light intensity ten times higher than was normally used were performed. Average swimming velocities of the cells $\langle V_z \rangle$, $\langle V_x \rangle$, $\langle V_p \rangle$ are plotted with open diamonds in Fig. 8A. The result of these experiments is that, even at a laser light intensity ten times greater than standard, no reliable evidence of phototaxis (i.e. a significant change in the cells' horizontal velocity $\langle V_x \rangle$) is detected. At the same time, the average vertical velocity component $\langle V_z \rangle$ (and thus $\langle V_p \rangle$) decreases faster than in the standard runs, and the standard deviation of cell velocity (Fig. 8B) for the runs with high light intensity significantly exceeds that for standard runs. Note that the standard deviations of V_z and V_x (triangles and stars in Fig. 8B) are now similar to the mean values of V_z and V_x. These findings can be associated with the influence of the laser light on the cell orientation mechanism.

The light-related responses (phototactic, photophobic and photokinetic) depend on the conditions under which the culture is grown, culture age, time of the day etc. Thus, measurements of the photokinetic response, and particularly the time it needs to develop, can be a sensitive indicator of the state of the cells' culture, which may be useful for biological applications.

Three-dimensional velocity distribution

Pedley and Kessler (1990) proposed the Fisher distribution to be an appropriate approximation for the three-dimensional cells' velocity distribution f in equation (9):

$$f(V,\theta) = R(V)e^{\lambda\cos\theta}\,, \qquad (10)$$

where R is some function of the forward velocity V. The

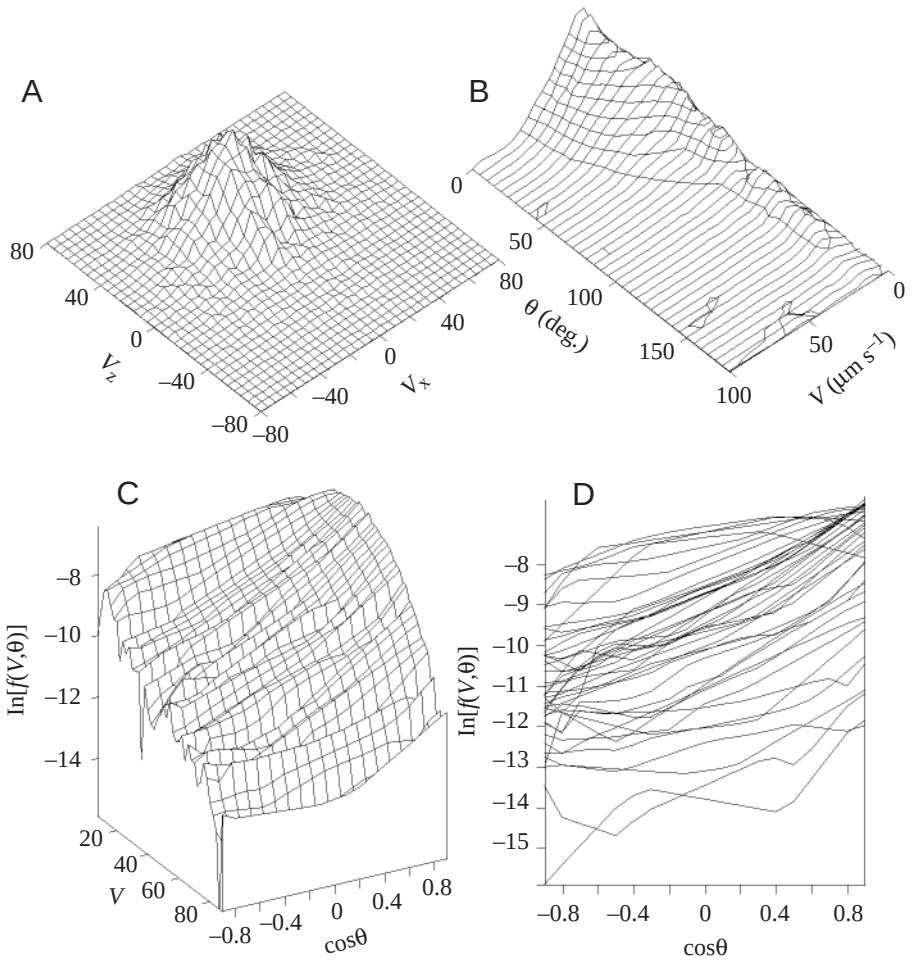

Fig. 10. Cell velocity distribution obtained on the basis of all tracks detected in all runs. (A) Surface plot of the two-dimensional probability density function $F(V_x,V_z)$; (B) surface plot of the reconstructed three-dimensional probability density function $F(V,\theta)$ (compare with Fig. 5); (C) surface plot of $\ln[f\,(V,\theta)]$; (D) sections of $\ln[f\,(V,\theta)]$ at different values of V, i.e. view of C from the tip of the V axis (compare with Fig. 11).

expression λcosθ is proportional to the gravitational potential energy of the bottom-heavy cell deviated from the equilibrium position, divided by this cell's rotational diffusivity. Thus, the exponential multiplier corresponds to the Boltzman distribution of the cells by the energy associated with their orientation. According to Equation 10, ln[$f(V,\theta)$] is predicted to be a linear function of cosθ with a slope λ. In Fig. 11, profiles of ln[$f(V,\theta)$] *versus* cosθ are presented for various values of V. In fact, these profiles are logarithmically re-scaled sections of the surfaces plotted in Fig. 5 on the planes $V = const$. Sections in the interval 30 μm s^{-1}<V<60 μm s^{-1} are plotted as bold lines. Within this restricted velocity range (bold lines), the graphs can be seen to be roughly linear, with λ in the range from 1.8 to 3.0, having the most typical value of 2.3. This is consistent with λ=2.2 suggested by Pedley and Kessler (1990). The value of λ recovered from the distributions for the entire population (Figs 9C, 10D) varies from 2 to 3, depending on θ, indicating that λ is not a constant but itself depends somewhat on θ.

One obvious interpretation of the absence of a uniquely defined value of λ is that, while cells obey the distribution (Equation 10), the culture contains organisms with different values of the 'bottom-heaviness' parameter λ.

Turning angle: random walk on circle

For a description of the cell swimming direction, Hill and Häder (1997) suggested a model of a biased random walk on a circle. To compare this model with the data obtained from our experiments, the mean and the variance of the cell turning angle E[θ(τ)–θ(0)] and Var[θ(τ)–θ(0)] are estimated and plotted *versus* time τ for tracks with different initial direction θ(0), where θ=0 corresponds to cells swimming vertically upward (Figs 12A, 13A). The averaging is performed over all 21-point tracks detected during all experimental runs. Each line corresponds to a group of cells with certain θ(0); in Fig. 13A, graphs are shifted vertically for convenience. Following Hill and Häder (1997), we approximate the graphs linearly for small enough τ to obtain the dependence of turning speed μ_0 (Fig. 12B) and rotational diffusivity σ_0 (Fig. 13B) on the cell orientation:

$$E[\theta(\tau) - \theta(0)] \sim \tau\mu_0[\theta(0)] , \quad (11)$$

$$Var[\theta(\tau) - \theta(0)] \sim \tau\sigma_0^2[\theta(0)] . \quad (12)$$

The function $\mu_0(\theta)$ (Fig. 12B) corresponds to the rate of returning of the pendulum (the bottom-heavy cell) to the equilibrium position (θ=0):

$$\mu_0(\theta) \sim -d_0 \sin\theta \sim -0.16 \sin\theta , \quad (13)$$

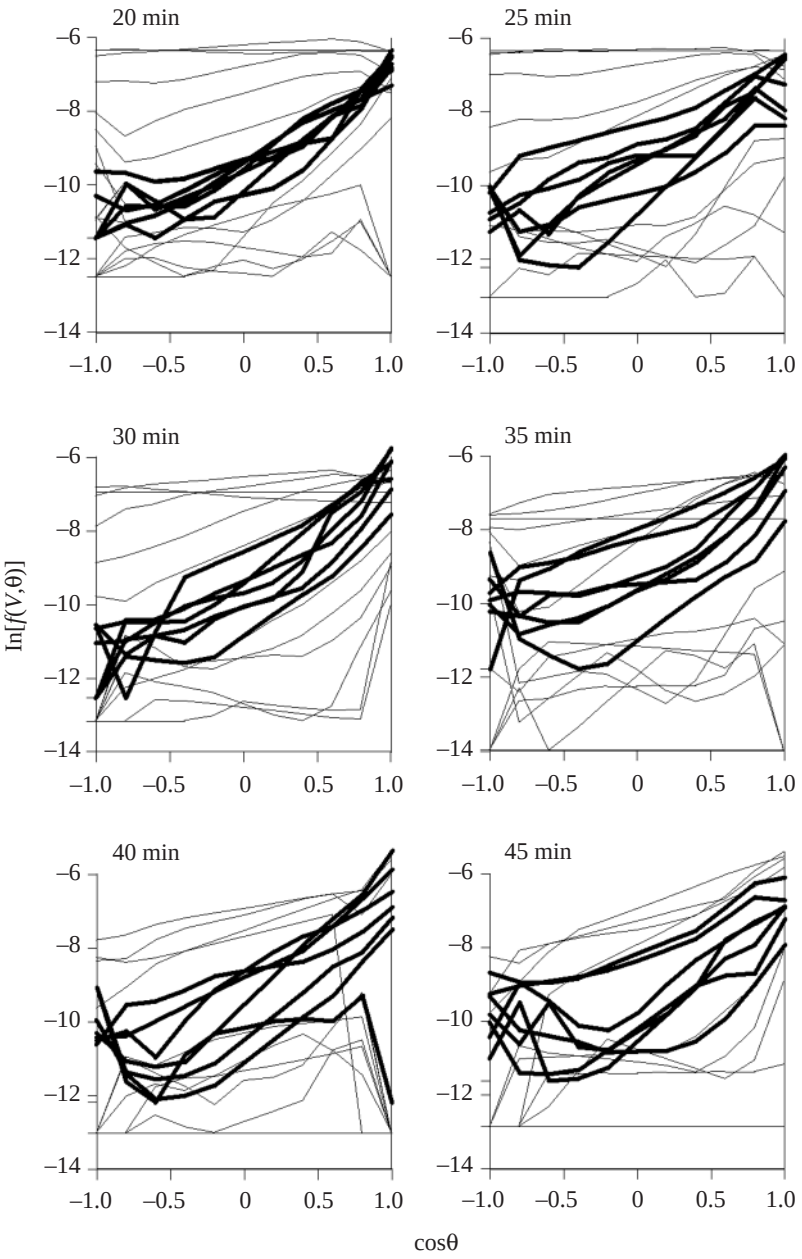

Fig. 11. Time evolution of the reconstructed three-dimensional cells' distribution by velocities (Equation 9). Cross-sections of ln[f (V,θ)] are plotted for different values of V. The slopes of the lines correspond to λ in Equation 10. Bold lines correspond to values of V between 30 μm s^{-1} and 60 μm s^{-1}.

where d_0 is the drift coefficient. This result is in reasonable agreement with that of Hill and Häder (1997), who reported a value of d_0 from 0.19 to 0.37 for different cultures.

The reorientation time B of a bottom-heavy cell in the field of gravity can be estimated theoretically from the balance between gravitational torque and the resisting viscous torque (Pedley and Kessler, 1987):

$$B = \frac{\mu\alpha_\perp}{2\rho g h} , \quad (14)$$

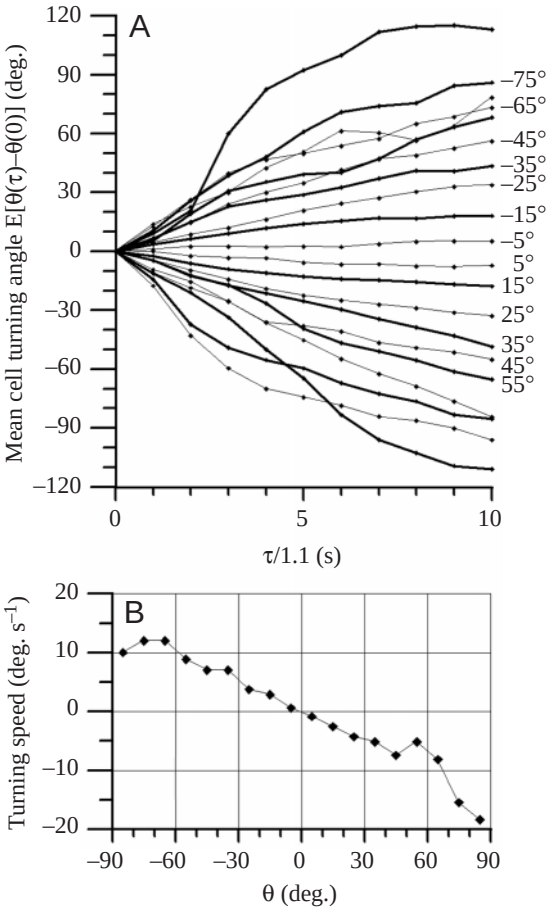

Fig. 12. (A) Averaged cell turning amplitude (Equation 11) *versus* time τ at different angles θ(0) from vertical; lines join points corresponding to θ(0)∈(0°,10°], θ(0)∈(10°,20°], θ(0)∈(20°,30°] etc; thin and bold lines are used to simplify visual comprehension. (B) Turning speed $\mu_0(\theta)$ *versus* angle, compare with Equation 13: gradient of the linear approximation to graphs in A for τ<5 s. See text for further explanation.

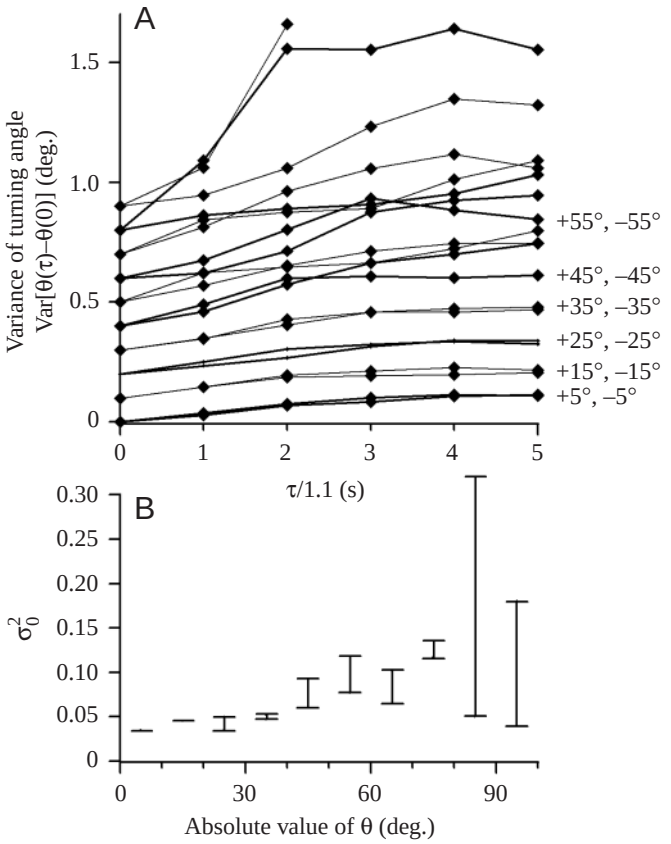

Fig. 13. (A) Variance of the turning amplitude (Equation 12) *versus* time τ for different angles from vertical θ(0); lines join points corresponding to θ(0)∈(0°,10°], θ(0)∈(10°,20°], θ(0)∈(20°,30°] etc. The origin of lines corresponding to different θ(0) are shifted vertically for convenience; thin and bold lines are used to simplify visual comprehension. (B) Rotational diffusivity $D_r=\sigma_0^2/2$ *versus* angle (Equation 12): gradients of the linear approximation to graphs in A for τ≤2 s. See text for further explanation.

where μ is the fluid viscosity, $\alpha_\perp\approx6.8$ is the dimensionless resistance coefficient, ρ is the cell density, $\boldsymbol{g}$ is the gravitational acceleration and h is the distance of the cell's centre of mass from its geometric centre. A guess of $h\approx0.1$ μm (Kessler, 1986) gives an estimate of $B\approx3.4$ s. A smaller value of h would result in larger B. Evaluated from our experiments, the drift coefficient (Equation 13) gives the reorientation time $B=d_0^{-1}\approx6$ s.

Solving the F–P equation for the cells' orientation, Pedley and Kessler (1990, 1992) showed that the constant λ in Equation 10 is related to B in Equation 14 by:

$$\lambda = \frac{1}{2BD_r}, \qquad (15)$$

where D_r is the rotational diffusivity, quantifying the directional randomness of the cells' trajectories. The observed value of λ=2.2 combined with B=6 s gives $D_r\approx0.04$ rad^2 s^{-1}. On the other hand, D_r is related to σ_0^2, defined in Equation 12 as $D_r=\sigma_0^2/2$. It is difficult to specify how σ_0^2 depends on θ because of the data scatter (Fig. 13). The value of σ_0^2 varies in the range 0.035–0.14, which corresponds to D_r in the range 0.018–0.07 rad^2 s^{-1}. This value is in agreement with the one estimated from Equation 15. However, our value of D_r is significantly smaller than 0.4–2.2 rad^2 s^{-1} estimated by Hill and Häder (1997). This may be caused by the difference in the experimental protocol: Hill and Häder observed all cells located in the experimental volume, while only upward swimming cells reach the observation area in our experiments. Berg (1983) suggested that the random reorientation of cells is due to rotational Brownian motion, but that gives an estimate $D_r\approx0.001$ rad^2 s^{-1} and, from Equation 15, the corresponding value of $B\approx200$ s, which is significantly larger than experimentally observed, confirming the customary view that Brownian effects on cells as big as 5 μm are insignificant.

Fig. 13B suggests that σ_0 and thus D_r increase with θ, which does not agree with the assumption that D_r is independent of

θ, as in the theory by Pedley and Kessler (1992b). One possible interpretation of the dependence of D_r on θ is the existence of some internal sensor of gravity in the cell, so that the reorientation mechanism is not entirely defined by the cell bottom-heaviness.

Autocorrelation of cell swimming direction

One characteristic illustrating the randomness of cell self-propulsion is the auto-correlation of its swimming direction. Assuming that all cells are identical (which is generally not true), we replace the time averaging by averaging over the ensemble:

$$\langle\theta(0),\theta(\tau)\rangle = \sum \theta(0)\theta(\tau) \cdot \left\{ \sum \theta(0)^2 \sum \theta(\tau)^2 \right\}^{-1/2}, \quad (16)$$

where θ is the deviation of the cells' swimming direction from the vertical and the time τ in Equation 16 is a discrete variable and can be written as τ=1.1 s × *n* where *n* = 0 to 17. Summations are performed over all 21-point tracks detected in a selected experimental run. The results are presented in Fig. 14 as separate curves on a semi-logarithmic plot. As mentioned above, a cell's velocity is derived from three successive displacements, so that θ(0) corresponds to displacement from the 1st to the 4th point and θ(17) corresponds to displacement from the 18th to the 21st point of the track. We observe that the auto-correlation of the cell swimming direction decreases exponentially with time, which is typical for stationary stochastic processes (Alt, 1989) and thus is consistent with the model of a random walk proposed in Hill and Häder (1997). The typical time of decay of the autocorrelation is around 10 s, i.e. the cell velocities within a 22 s burst are correlated and cannot be considered as statistically independent. That is the reason why only one segment of each track is used to construct the cells' velocity distribution and to calculate the average velocities. It is worth noticing that the auto-correlation of the cell swimming direction for the run that turned out to be invalid (see Appendix) differs from that related to the normal runs (broken line in Fig. 14).

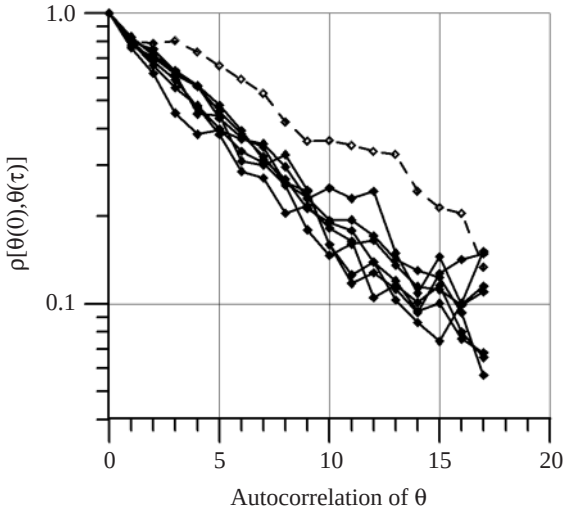

Fig. 14. Autocorrelation of the cells' swimming direction (projected onto the *x–z* plane) calculated for the tracks detected in seven experimental runs separately (Equation 16). The broken line corresponds to the run that turned out to be invalid. Solid lines connect points related to one run. The exponential decrease of correlation with time τ is typical for random walk processes.

Final remarks

The technique presented above allows us to study the parameters of micro-organism self-swimming by averaging among hundreds of micro-organisms. The spatial and temporal dependence of micro-organism motility can be studied, which is useful for understanding various types of taxis and bioconvection phenomena.

Deviations of the observed cell swimming behaviour from the biased random walk, together with the increase of scatter in the cells' velocities at high laser light intensity, can be associated with the existence of some internal cell orientation mechanism. No reliable conclusions can be reached at this stage, so further studies of the evolution of the cell swimming direction will be conducted.

A study of cell self-swimming may be interesting from the biological point of view: cell motility and light-related responses can be used as sensitive indicators of the cells' physiological state. In particular, faster/slower-swimming cells, or cells with stronger/weaker gravitactic, phototactic and photokinetic properties can be distinguished. Sometimes a difference between cell cultures can be visually observed by comparing composed images of swimming cells such as Fig. 2B. As the next step, an investigation of the influence of various environmental parameters on the self-swimming of various micro-organisms will be conducted using the technique described above.

Appendix

The hypothesis to test is the following:

At any time instant, the measured number of cells $n_{r,b,ij}$ in the bin *(i,j)* defined by Equation 2 is distributed in accordance with the averaged distribution $\bar{F}_{i,j}(\tau)$ defined by Equation 5.

If the answer is positive, we get evidence of the absence of any hidden parameters in the experiments. The χ^2 test for the multinomial distribution is applied as described by Ostle and Malone (1988). Consider the deviation $\zeta_{r,b}$ of the number of cells $n_{r,b,ij}$ detected in the bin (*i,j*) during the burst *b* of the run *r* from that expected in accordance with the distribution $\bar{F}_{i,j}$ at the time instant $t_{r,b}$:

$$\xi_{r,b} = \sum_{\bar{n}_{r,b,ij} \geq 3} \left(\frac{(\bar{n}_{r,b,ij} - n_{r,b,ij})^2}{\bar{n}_{r,b,ij}} \right) + \zeta_{r,b}, \quad (A1)$$

where $\bar{n}_{r,b,ij}$ is the expected number of events in the bin (*i,j*) detected during burst *b* of run *r*:

$$\bar{n}_{r,b,ij} = \bar{F}_{i,j}(t_{r,b}) N_{r,b}, \quad (A2)$$

and $\zeta_{r,b}$ is the term corresponding to bins with $\bar{n}_{r,b,ij}<3$ that are

merged to form larger ones, as it is common to do for the multinomial distribution. The summation in Equation A1 is performed over all bins with $\bar{n}_{r,b,ij} \geqslant 3$. If the hypothesis mentioned above is correct, the quantity $\xi_{r,b}$ is a random variable exhibiting a χ^2 distribution with $\nu_{r,b}$ degrees of freedom. Here:

$$\nu_{r,b} = k_{r,b} - 1 + \sum_{\bar{n}_{r,b,ij} \geq 3} 1 , \qquad \text{(A3)}$$

where $k_{r,b}$ is the number of bins composed from those with the expected number of cells less than 3. Introduce the probabilities $p_{r,b}$:

$$p_{r,b} = P(\xi > \xi_{r,b} : \nu_{r,b}) = 1 - \chi^2_{(\nu_{r,b})}(\xi_{r,b}) , \qquad \text{(A4)}$$

and it is easy to show that, given that the hypothesis is true, the values $p_{r,b}$ must be homogeneously distributed in the interval [0,1). To test this fact, the Kolmogorov–Smirnov criterion is applied as described by Blum and Rosenblatt (1972). To demonstrate that the result is not too sensitive to the choice of the parts of the tracks being analyzed, the data based on the beginnings of the tracks and the data based on the ends of the tracks are considered separately. The maximum differences of the measured distributions (Equation A4) from the uniform distribution are 0.22 and 0.19. These correspond to confidence levels of 0.76% and 2.6%, which are significant, so we conclude that the hypothesis is invalid.

Examining each of the experimental runs separately, we found that the distribution obtained from one of them differs from the averaged distribution by more than the others. Also, autocorrelation of the cell's swimming direction in this run significantly deviates from that in other runs (the broken line in Fig. 14). This could have happened because some uncontrolled deviation in experimental procedure appeared during this run, making it invalid. We eliminated that particular run from the data and repeated the averaging procedure (Equation 5). Now the maximum differences of distribution of $p_{r,b}$ from the uniform distribution become 0.09 and 0.10, which gives insignificant confidence levels of 92% and 82%. Thus we have a set of seven reliably similar experimental runs, which contain 47 bursts with 8794 tracks detected.

List of symbols and abbreviations

B	cell reorientation time in the gravity field
b	burst number
b_n, b_{n+1}	brightness of the blob interpreted as the cell image in frames n and n+1
D_r	cell rotational diffusivity
d_0	angular drift coefficient
f	three-dimensional velocity distribution
F	two-dimensional velocity distribution
FP	Fokker–Planck
$\boldsymbol{g}$	gravitational acceleration
h	distance of the cell's centre of mass from its geometric centre
$n_{r,b,ij}$	number of cells detected in the burst b of the run r in the bin with a particular velocity
$N_{r,b}$	total number of cells detected in the burst b of the run r
p.d.f.	probability density function
r	run number
$t_{r,b}$	time when the burst b of the run r has been acquired
$V_{x/z/p}$	horizontal/vertical/projected velocity
v_n	magnitude of the velocity vector $\vec{v}_n$
$\vec{v}$	cell velocity derived from the difference of its position in sequential images
w	weight
$\alpha_\perp$	dimensionless resistance coefficient
θ	deviation of cell swimming direction from vertical
λ	gravitaxis constant
σ_0^2	doubled rotational diffusivity
ρ	cell density
τ	time
μ	fluid absolute (dynamic) viscosity
μ_0	turning speed

The authors thank Prof. N. A. Hill and Prof. J. O. Kessler for useful discussions. This research forms a part of the Hull Institute for Mathematical Science and Applications (HIMSA) programme on 'The Self-Swimming of Micro-Organisms' and was supported by a start-up grant (for Prof. V. A. Vladimirov's research group) from the University of Hull and by a joint UK/HK grant (with Prof. M. Wu).

References

Alt, W. (1989). Correlation analysis of two-dimentional locomotion path. In *Lecture Notes in Biomathematics* **89** (ed. W. Alt and G. Hoffmann), pp. 254-268. Berlin, Heidelberg: Springer-Verlag.

Bees, M. A. and Hill, N. A. (1997). Wavelengths of bioconvection patterns. *J. Exp. Biol.* **200**, 1515-1526.

Berg, H. C. (1983). *Random Walks in Biology*. Princeton: Princeton University Press.

Blum, J. R. and Rosenblatt, J. I. (1972). *Probability and Statistics*. Philadelphia (PA): Saunders.

Chandrasekhar, S. (1943). Stochastic problems in physics and astronomy. *Rev. Mod. Phys.* **15**, 1-89.

Childress, S., Levandowsky, M. and Spiegel, E. A. (1975). Pattern formation in a suspension of swimming microorganisms: equations and stability theory. *J. Fluid Mech.* **63**, 591-613.

Fasham, M. J. R., Ducklow, H. W. and McElvie, S. M. (1990). A nitrogen based model of plankton dynamics in the ocean mixed layer. *J. Mar. Res.* **48**, 591-639.

Gorenflo, R. and Vessela, S. (1991). Abel Integral Equations. *Lecture Notes in Mathematics* **1461**. Berlin, Heidelberg, New York, Tokyo: Springer-Verlag.

Harris, E. H. (1989). *Chlamydomonas Source Book*. New York, London: Academic Press.

Hill, N. A. and Häder, D.-P. (1997). A Biased Random Walk Model for the Trajectories of Swimming Micro-organisms. *J. Theor. Biol.* **186**, 503-526.

Kessler, J. O. (1985). Hydrodynamic focussing of motile algal cells. *Nature* **313**, 218-220.

Kessler, J. O. (1986). Individual and collective dynamics of swimming cells. *J. Fluid Mech.* **173**, 191-205.

Kessler, J. O., Hoelzer, M. A., Pedley, T. J. and Hill, N. A. (1994). Functional patterns of swimming bacteria. In *Mechanics and Physiology of Animal Swimming* (ed. L. Maddock, Q. Bone and J. M. V. Rayner), pp. 3-12. Cambridge: Cambridge University Press.

Kessler, J. O., Hill, N. A. and Häder, D.-P. (1992). Orientation of swimming flagellates by simultaneously acting external factors. *J. Phycol*. **28**, 816-822.

Matsunaga, S., Takahashi, T., Watanabe, M., Sugai, M. and Hori, T. (1999). Control by ammonium ion of the change from step-up to step-down photophobically responding cells in the flagellate alga *Euglena gracilis*. *Plant Cell Physiol.* **40**, 213-221.

Matthews, L. M. and Brindley, J. (1997). Patchiness in plankton populations. *Dyn. Stab. Syst.* **12**, 39-59.

Nikolai, H., Herzhaft, B., Hinch, E. J. et al. (1995). Particle velocity fluctuations and hydrodynamic self-diffusion of sedimenting non-Brownian spheres. *Phys. Fluids* **7**, 12-23.

Ostle, B. and Malone, L. C. (1988). *Statistics in Research, Basic Concepts and Techniques for Research Workers.* Ames (Iowa, USA): Iowa State University Press.

Pedley, T. J. and Kessler, J. O. (1987). The orientation of spheroidal micro-organisms swimming in a flow field. *Proc. R. Soc. Lond. B* **231**, 47-70.

Pedley, T. J. and Kessler, J. O. (1990). A new continuum model for suspension of gyrotactic micro-organisms. *J. Fluid Mech.* **212**, 155-182.

Pedley, T. J. and Kessler, J. O. (1992a). Bioconvection. *Sci. Progress* **76**, 105-123.

Pedley, T. J. and Kessler, J. O. (1992b). Hydrodynamic phenomena in suspensions of swimming microorganisms. *Annu. Rev. Fluid Mech.* **24**, 313-358.

Platt, J. R. (1961). 'Bioconvection patterns' in cultures of free-swimming organisms. *Science* **133**, 1766-1767.

Truscott, J. E. and Brindley, J. (1995). Environmental forcing of simple plankton models. *J. Plankton Res.* **17**, 2207-2232.

Vladimirov, V. A., Denissenko, P. V., Pedley, T. J., Wu, M. and Moskalev, I. S. (2000). Algal motility measured by a laser-based tracking method. *Mar. Freshwater Res.* **51**, 589-600.

Wager, H. (1911). On the effect of gravity upon the movements and aggregation of *Euglena viridis*, EHRB., and other micro-organisms. *Phil. Trans. R. Soc. Lond. B* **201**, 333-390.